RCTA
Revista Colombiana de Tecnologías de Avanzada
UNIPAMPLONA

Design, implementation, and functional validation of a short-range LoRa-based underwater monitoring architecture

Diseño, implementación y validación funcional de una arquitectura de monitoreo subacuático de corto alcance basada en LoRa

Ing. Diego Arbey Montezuma Rosero[1], **MSc. Fabián Geovanny Cuzme Rodríguez**[1], **MSc. Jaime Roberto Michilena Calderón**[1], **MSc. Luis Edilberto Suárez Zambrano**[1]

[1] **Universidad Técnica del Norte,** Facultad de Ingeniería en Ciencias Aplicadas, Av. 17 de Julio 5-21 y General José María Córdova, Ibarra 100105, Ecuador.

Correspondence: fgcuzme@utn.edu.ec

Received: may 26, 2026. **Revised:** june 26, 2026. **Accepted:** july 31, 2026. **Published:** august 04, 2026.

How to cite: D. A. Montezuma Rosero, F. G. Cuzme Rodríguez, J. R. Michilena Calderón, and L. E. Suárez Zambrano, "Design, implementation, and functional validation of a short-range LoRa-based underwater monitoring architecture", *Revista Colombiana de Tecnologías de Avanzada (RCTA)*, vol. 2, no. 48, pp. 209–224, Aug. 2026, doi: 10.24054/rcta.v2i48.4509

Abstract: Environmental monitoring in aquatic ecosystems requires communication systems capable of operating under the particular conditions of underwater environments. This work presents the design, implementation, and functional validation of a short-range underwater monitoring system based on LoRa technology for freshwater environments. The developed architecture integrates a submerged sensor node for environmental data acquisition, a communication buoy located at the water surface, and a web platform for real-time data visualization. Communication between the sensor node and the buoy is performed through a LoRa link operating in the 915 MHz ISM band under an underwater-to-overwater (UW2OW) configuration, while data transmission to the cloud is carried out through a 2.4 GHz Wi-Fi connection. Functional validation was conducted in a controlled environment consisting of a swimming pool and in natural freshwater environments represented by two lagoons, considering different node depths and horizontal separation distances. The maximum distance with detectable reception depended on the node depth and the test environment, ranging from 1.2 to 13 m. However, packet loss increased considerably near these limits; therefore, more conservative operational reference distances were established. Operational limitations related to node depth, packet loss, transmission delay, and effective receiver sensitivity were also identified. The results demonstrate the functional feasibility of the proposed architecture for low-dynamic environmental monitoring applications and provide an experimental basis for future improvements to the communication system and deployment mechanisms in aquatic environments.

Keywords: underwater communication, LoRa, environmental monitoring, wireless sensor networks, telemetry.

Resumen: El monitoreo ambiental en ecosistemas acuáticos requiere sistemas de comunicación capaces de operar bajo las condiciones particulares del medio subacuático. En este trabajo se presenta el diseño, implementación y validación funcional de un sistema de monitoreo subacuático de corto alcance basado en la tecnología LoRa para ambientes de agua dulce. La arquitectura desarrollada integra un nodo sensor sumergido para la adquisición de variables ambientales, una boya de comunicaciones ubicada en superficie y una plataforma web para la visualización de la información en tiempo real. La comunicación entre el nodo sensor y la boya se realiza mediante un enlace LoRa en la banda ISM de 915 MHz bajo una configuración underwater-to-overwater (UW2OW), mientras que la transmisión hacia la nube se efectúa mediante Wi-Fi a 2.4 GHz. La validación funcional se realizó en un entorno controlado (piscina) y en ambientes naturales (lagunas de agua dulce), evaluando el comportamiento operativo del sistema bajo diferentes profundidades y distancias de separación entre el nodo y la boya. Los resultados muestran que la distancia máxima con recepción detectable dependió de la profundidad y del escenario evaluado, con valores comprendidos entre 1.2 y 13 m. No obstante, la pérdida de paquetes aumentó considerablemente al aproximarse a estos límites, por lo que se establecieron distancias operativas de referencia más conservadoras. Asimismo, se identifican limitaciones operativas asociadas con la profundidad, la pérdida de paquetes, el retardo de transmisión y la sensibilidad efectiva del sistema, aspectos que deben considerarse durante el despliegue de este tipo de soluciones. Los resultados obtenidos demuestran la factibilidad funcional de la arquitectura propuesta para aplicaciones de monitoreo ambiental de baja dinámica y proporcionan una base experimental para futuras optimizaciones del sistema de comunicación y de los mecanismos de despliegue en ambientes acuáticos.

Palabras clave: comunicación subacuática, LoRa, monitoreo ambiental, redes de sensores inalámbricos, telemetría.

1. INTRODUCTION

Underwater communications have experienced significant development in recent years [1]. Nevertheless, their implementation remains challenging because the propagation characteristics of the medium impose limitations related to bandwidth, propagation speed, data transfer rate, device power supply, and the complexity of infrastructure deployment [2]. To address these constraints, underwater communication systems have been developed mainly through acoustic, optical, and electromagnetic approaches. Acoustic communication is one of the most widely used approaches in underwater environments because sound waves can propagate over long distances in water. However, its performance may be limited by ambient noise, latency, energy consumption, and variations in the aquatic medium [3]. Optical communication, on the other hand, supports high data rates but requires favorable alignment and visibility conditions. Light absorption, scattering, and water turbidity considerably reduce its communication range [4].

The third approach is electromagnetic communication based on radio-frequency signals, which is the focus of this study. Electromagnetic waves offer advantages associated with low latency and the possibility of using compact communication devices; however, they experience significant attenuation when propagating through aquatic media, particularly as the operating frequency, water conductivity, and device depth increase [5]. Consequently, their application is primarily oriented toward short-range underwater links. LoRa technology employs a chirp-based spread-spectrum modulation scheme known as Chirp Spread Spectrum (CSS) [6] and was developed for long-range, low-power wireless communications [7]. Its high receiver sensitivity and robust modulation make it a potential candidate for short-range underwater links. Nevertheless, its performance in these environments depends on the characteristics of the aquatic medium, depth, operating frequency, radio configuration, and physical implementation of the antennas.

This work proposes the design and implementation of a short-range underwater monitoring system based on LoRa technology for freshwater environments. The architecture integrates a submerged sensor node responsible for acquiring environmental variables, a communication buoy located at the water surface to receive and retransmit the information, and a web platform for data storage and visualization. The study focuses on the functional validation of the complete architecture in controlled and natural environments, considering the operational limitations observed during deployment [8].

Within the scope of this research, previous studies involving experimental tests with communication nodes deployed in aquatic environments were identified. One such study proposed the use of the 433 MHz frequency band through TWS-433 RF transmitter and receiver modules. Two nodes were positioned above the water surface under an overwater-to-overwater (OW2OW) configuration, achieving a maximum signal propagation distance of up to 9 m [5].

Another study used higher frequencies to evaluate data transmission in an underwater environment, with both the transmitter and receiver placed at a depth of 0.15 m. Under these conditions, data transfer was achieved over a distance of up to 0.16 m in the 2.4 GHz frequency band [3]. Bluetooth technology, which operates in the same frequency band, has also been evaluated in a fish-tank test environment containing both freshwater and saltwater. In that study, two nodes separated by a few centimeters under an underwater-to-overwater (UW2OW) configuration achieved a propagation distance of up to 0.19 m [4].

Regarding the use of LoRa technology, a study conducted at Dishui Lake in Shanghai employed the 433 MHz frequency band with similar Spreading Factor and bandwidth parameters. Three communication configurations were evaluated: submerged transmitter and submerged receiver (UW2UW), submerged transmitter and receiver at the water surface (UW2OW), and transmitter at the water surface and submerged receiver (OW2UW). The results showed that links involving one submerged node and one surface node provided the best performance [9].

Other studies have focused on the design of antennas for LoRa communication at 868 MHz, achieving a transmission distance of 0.6 m when both nodes were submerged in water [10].

In a subsequent study, Pozzebon et al. evaluated LoRaWAN transmissions from water to the surface through laboratory and field tests conducted in saltwater. The results showed that reception could be maintained when the transmitter was located at a shallow depth, although reliability decreased considerably as the receiver sensitivity limits were approached. This study confirms the importance of distinguishing between detectable reception and reliable operation in aquatic applications [11].

Although previous studies have demonstrated the feasibility of using radio-frequency signals and LoRa technology for short-range underwater communications, most investigations have focused on analyzing the behavior of the physical link or evaluating isolated communication modules. In contrast, few studies have presented an integrated environmental monitoring architecture combining an underwater sensor node, a LoRa–Wi-Fi communication buoy, and a remote monitoring platform validated through experimental tests in real freshwater environments. This research gap motivates the development of the system presented in this work.

In this context, the main contribution of this research is the design, implementation, and functional validation of a short-range LoRa-based underwater monitoring architecture. The specific contributions include: i) the implementation of a submersible sensor node for environmental variable acquisition; ii) the development of a buoy integrating LoRa and Wi-Fi communications for cloud data transmission; iii) the integration of a web platform for information storage and visualization; and iv) the functional validation of the system in controlled and natural environments, identifying operational limitations associated with depth, packet loss, delay, and the effective sensitivity of the prototype.

The remainder of this paper is organized as follows. Section 2 describes the proposed architecture, the materials used, and the experimental methodology employed for the design, implementation, and validation of the system, as well as the simulation model used as a reference. Section 3 presents the experimental results obtained in the different evaluation scenarios. Section 4 discusses the results and compares them with related studies, analyzing the main limitations and scope of the proposed system. Finally, Section 5 presents the conclusions and future research directions.

2. METHODOLOGY

2.1. System Desing

The system was implemented using two Heltec Wi-Fi LoRa 32 V3 boards, which integrate an ESP32-S3 microcontroller and LoRa, Wi-Fi, and Bluetooth connectivity. One board was used in the sensor node, while the second was installed in the communication buoy. The sensor node acquires pH and turbidity measurements and transmits the information via LoRa at 915 MHz to the buoy located at the water surface. The buoy then retransmits the data via Wi-Fi to Firebase for storage and visualization through a web platform.

The architecture consists of three main elements: i) a sensor node submerged at the depth defined for each test; ii) a communication buoy that receives the packets under an underwater-to-overwater (UW2OW) configuration; and iii) a web platform for remote data storage and visualization. LoRa communication is established through a point-to-point link between the two Heltec boards, whereas the Wi-Fi connection is used exclusively between the buoy and the cloud platform.

The Heltec Wi-Fi LoRa 32 V3 board was selected because it integrates the SX1262 transceiver and the ESP32-S3 microcontroller into a single device, supports a transmission power of up to 21 dBm, and can be programmed using the Arduino IDE. Its main technical specifications are summarized in Table 1.

Table 1: *Technical Specifications of the Heltec WiFi LoRa 32 V3 Development Board*

	Specifications
Microcontroller	ESP32
LoRa Chip	SX1262
Power Consumption	<10 µA
Operating Frequency	863–928 MHz / 470–510 MHz
Maximum Transmission Power	21 ± 1 dBm
Maximum Sensitivity	−137 dBm
Integrated Technologies	Bluetooth, Wi-Fi, LoRa
Operating Temperature	−20 °C to 70 °C
Operating Voltage	3.7 V

Fuente: *Heltec Platform [12] and Semtech [20]*

The LoRa transmission parameters were configured to prioritize communication range and signal robustness under harsh operating conditions, as these settings directly affect link performance. Transmission speed and data rate are closely related to the Spreading Factor.

In its highest configuration, SF12 increases signal robustness against interference, extends the communication range, and improves receiver sensitivity, although at the expense of a lower data rate. Similarly, the Coding Rate introduces additional redundancy bits for error correction, which is particularly useful in environments characterized by high packet-loss levels. A low bandwidth of 125 kHz was also selected to improve communication range, although this configuration reduces the achievable data throughput.

The communication parameters considered in this study were operating frequency, transmission power, bandwidth, Spreading Factor, Coding Rate, and preamble length. All parameters were configured to favor greater signal robustness and extended communication range. The selected values are summarized in Table 2.

Table 2: *Configured Transmission Parameters*

	Configuration
Frequency	915 MHz
Transmission Power	21 dBm
Bandwidth	125 kHz
Spreading Factor	12
Coding Rate	4/8
Preamble Length	12 symbols

Source: *own elaboration.*

2.1.1. System Architecture

Considering the configuration parameters selected for the Heltec Wi-Fi LoRa 32 V3 board, a system was designed to monitor an underwater environment through the implementation of the two previously described nodes. LoRa is used for communication in the underwater environment, while Wi-Fi is used to transmit the data to the Firebase database, where the information is stored and subsequently displayed in real time through a web platform.

The process begins with the sensor node, which is submerged to the depth defined for each test and is equipped with sensors that measure environmental variables such as water pH and turbidity. The node processes the acquired information in real time and transmits it in the 915 MHz band to a communication buoy located at the water surface, which is equipped with a receiving antenna configured at the same frequency. Because electromagnetic signals experience high attenuation in aquatic media, the buoy operates as a nearby relay that receives the LoRa signal from the submerged node and retransmits the information through a 2.4 GHz Wi-Fi link. Once the data are received, the buoy uses the Wi-Fi connectivity integrated into the Heltec Wi-Fi LoRa 32 V3 board to establish an Internet connection and send the information to Firebase in real time.

A user monitoring the system can access the data through a web interface connected to the Firebase database. The platform retrieves the stored information and displays it through graphical representations that facilitate its interpretation, enabling continuous monitoring of water conditions. The overall system architecture is shown in Fig. 1.

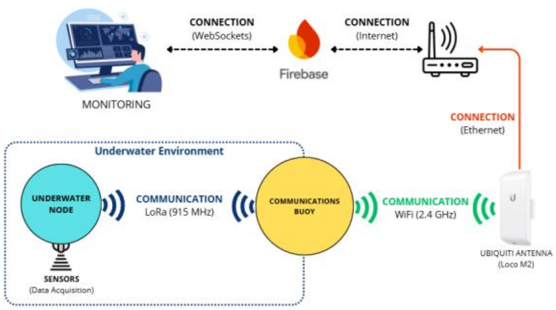

Fig. 1. *System Architecture.*
Source: *own elaboration.*

2.1.2. System Functionality

The complete system workflow is shown in Fig. 2, which illustrates the interaction among its different components to achieve environmental variable monitoring through LoRa communication.

Both the sensor node and the communication buoy execute an initialization stage. During this stage, the communication parameters are configured, the hardware is activated, and the processes required for system startup are executed. Once both devices have been initialized, the sensor node reads the data provided by the sensors in contact with the water. These data are temporarily stored in the flash memory of the Heltec Wi-Fi LoRa 32 V3 board using internal variables. Subsequently, a structured data packet containing all the information is generated as a text string. Before transmitting the data string, the system verifies, during the first startup, whether the buoy is available to receive packets. If the receiver responds positively, the transmission process begins. The sensor node periodically checks whether the buoy remains online to avoid unnecessary packet transmissions. Each time a packet is transmitted, a function releases the LoRa communication module so that it is available for the next transmission, while an LED is activated to indicate that the packet has been sent.

Regarding the communication buoy, once the system has started, it establishes a connection to the Wi-Fi network. After the connection is successfully established, a request is sent to an NTP server to synchronize the current time. The buoy then connects to the Firebase database and remains in a waiting state until packets are received through the LoRa module. When a packet arrives, the indicator LED is activated, and the packet is stored as a text string in the flash memory. The individual values are then extracted and stored in separate variables while being simultaneously displayed on the OLED screen of the Heltec Wi-Fi LoRa 32 V3 board.

Finally, the data are transmitted to Firebase for both historical storage and real-time updating. Once this process is completed, the system returns to standby mode and waits for new data. The user interface, implemented as a web page, sends requests to Firebase to retrieve the updated values. These data are displayed through historical graphs and can also be visualized in real time as they are received from the system, as shown in Fig. 2.

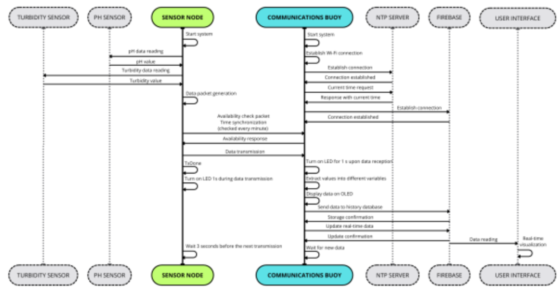

Fig. 2. *System sequence diagram.*
Source: *own elaboration.*

2.1.3. Sensor Node Design

The sensor node is the most exposed component of the system because it must operate while submerged at a defined depth; therefore, its electronic components require watertight protection. As shown in Fig. 3, the node integrates pH and turbidity sensors, signal-conditioning modules, a Heltec Wi-Fi LoRa 32 V3 board, and a LoRa antenna connected through the U.FL interface. The board receives, processes, and transmits the data acquired by the sensors through the ESP32 pins. The system is powered by a 3.7 V battery and uses a 3.7-to-5 V converter to supply the voltage required by the sensors.

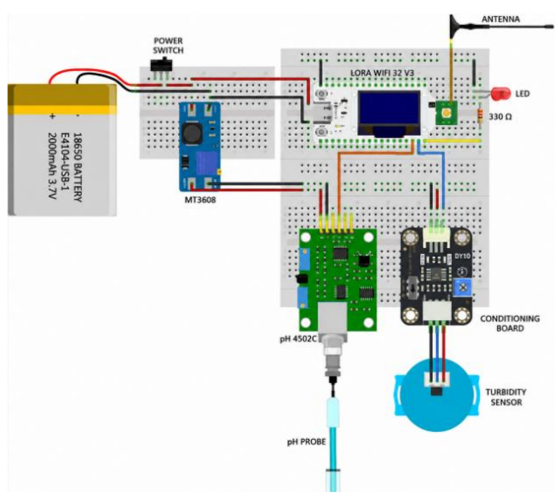

Fig. 3. *Electronic module connection diagram (Sensor Node).*
Source: *own elaboration.*

The electronic components of the sensor node are housed in a watertight enclosure designed using 3D modeling to protect them against water ingress during underwater tests. The spherical structure is divided into upper and lower sections, joined by an intermediate threaded connection that provides access to the interior and facilitates system assembly and maintenance.

The upper section includes a compartment for the lithium-polymer battery, a mounting base for the PCB, an external handle for securing and retrieving the node using ropes, and protected openings for the LED indicator and the LoRa antenna. These elements were designed to maintain the watertight integrity of the enclosure and protect both the electronic components and the connections exposed to the aquatic environment, as shown in Fig. 4.

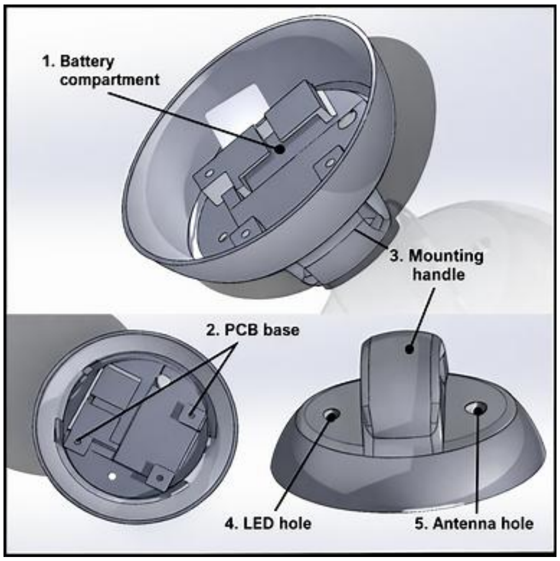

***Fig. 4**. Upper cover design (Sensor Node).*
***Source:** own elaboration.*

The lower cover of the spherical enclosure, shown in Fig. 5, is intended for sensor integration and control of the node's immersion. This section incorporates attachment rings and cavities for adding weights, a threaded connection to the upper cover, and a central protective cylinder. It also includes threaded openings for the secure installation of the pH and turbidity sensors while maintaining the mechanical protection and watertight sealing of the enclosure.

***Fig. 5**. Lower cover design (Sensor Node).*
***Source:** own elaboration.*

2.1.4. Communication Buoy Design

The electronic design of the communication buoy is centered on the Heltec Wi-Fi LoRa 32 V3 module. In this case, the connection scheme is simpler, as the board is powered by a 3.7 V battery. The integrated LoRa transceiver receives the data through the LoRa antenna operating at 915 MHz and retransmits them to Firebase using the Wi-Fi module integrated into the ESP32 microcontroller, as shown in Fig. 6.

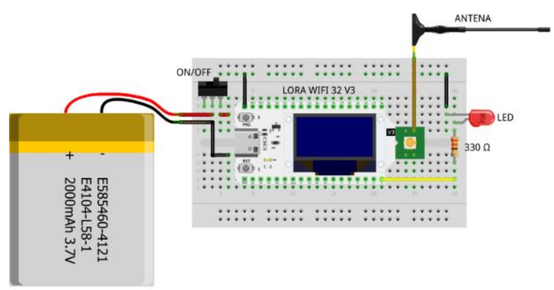

***Fig. 6**. Electronic module connection diagram (Communication Buoy).*
***Source:** own elaboration.*

2.1.5. Web Platform Design

The data visualization platform was implemented using Firebase because it enables real-time synchronization among the devices connected to the platform. As a NoSQL database, Firebase stores the information in JSON format [13]. The database used in this system contains eight branches, each storing information in separate variables. Two data categories were defined: historical data and real-time data. The overall database structure is shown in Fig. 7.

ISSN: 1692-7257 - Volume 2 – Number 48 - 2026

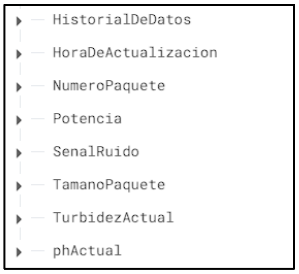

Fig. 7*. Firebase data tree structure.*
Source: *own elaboration.*

A branch named "HistorialDeDatos" was created to store the information received from the communication buoy as a historical record. Each entry is indexed by a timestamp and contains a structured set of all the collected data, which enables the subsequent generation of historical plots, as shown in Fig. 8(a). In contrast, the real-time data are stored as individual variables that are automatically updated whenever new information is uploaded to the platform from the buoy, as shown in Fig. 8(b).

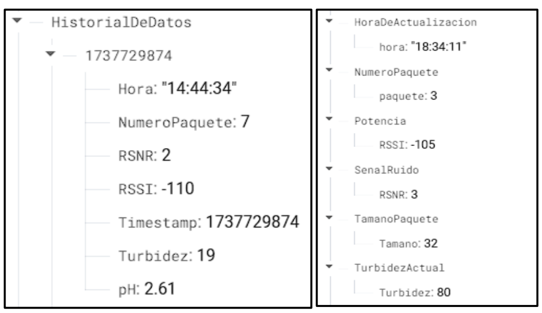

(a) *(b)*

Fig. 8*. Historical data (a) and real-time data (b) retrieved from Firebase.*
Source: *own elaboration.*

The user interface was implemented as a web application developed using HTML, CSS, and JavaScript. The platform retrieves the two types of data stored in Firebase, namely historical and real-time data. As shown in Fig. 9, the information is displayed through web-based data cards whose values are updated in real time as new data are synchronized with Firebase.

Fig. 9*. Real-time data visualization cards.*
Source: *own elaboration.*

Another method of presenting the information on the web platform is through historical plots, which allow users to observe how the data evolve over time. For this purpose, the data structure generated under the "HistorialDeDatos" branch in Firebase is used, as shown in Fig. 10.

Fig. 10*. Historical data visualization graph.*
Source: *own elaboration.*

2.2. Implementation

2.2.1. Sensor Node

The construction of the sensor node, which houses the electronic components and sensors, was carried out using the previously described 3D-printed design. The enclosure provides a watertight structure to protect the components in the aquatic environment. The design includes four openings: two for the sensors in direct contact with the water, one for the LoRa antenna, and one for the LED operation indicator. The implemented internal and external structure is shown in Fig. 11.

(a) *(b)*

Fig. 11*. Sensor node, internal (a) and external (b) views.*
Source: *own elaboration.*

2.2.2. Communication Buoy

The communication buoy, which houses the electronic components, was constructed using a buoyant material, specifically polystyrene. The LoRa antenna is positioned at the water surface, while the module's 2.4 GHz antenna is used to establish the Wi-Fi connection to the Internet. The buoy design is shown in Fig. 12. An outdoor watertight electrical enclosure with an IP65 protection rating was used to protect the internal components against dust ingress and water jets [14].

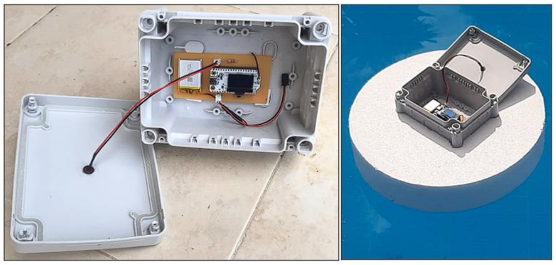

(a) *(b)*

Fig. 12. *Communication buoy, internal (a) and external (b) views.*
Source: *own elaboration.*

2.3. Experimental Protocol

The tests were organized according to the evaluation scenario, the depth of the sensor node, and the horizontal distance between the submerged node and the communication buoy. For each combination of scenario, depth, and distance, two independent tests were conducted. In each test, 50 packets were transmitted with a 10 s interval and a payload size of 60 bytes. The LoRa configuration remained constant throughout all tests: a carrier frequency of 915 MHz, a transmission power of 21 dBm, a bandwidth of 125 kHz, SF12, CR 4/8, and a preamble length of 12 symbols.

For each successfully received packet, the packet identifier, RSSI, SNR, payload size, and timestamps used to calculate the delay were recorded. The reported delay corresponds exclusively to the data transfer between the sensor node and the buoy. It was calculated as the difference between the timestamp assigned to the packet when it was transmitted by the sensor node's LoRa module and the timestamp recorded when the packet was received by the buoy. Before each test, the clocks used by the sensor node and the buoy were synchronized through an NTP server, as illustrated in Fig. 2. The packet error rate was calculated using (1).

$$PER = \frac{N_{tx} - N_{rx}}{N_{tx}} \tag{1}$$

where N_{tx} is the number of transmitted packets and N_{rx} is the number of packets successfully received. For RSSI, SNR, and delay, the mean and standard deviation were calculated using the packets received under each experimental condition. Two concepts were distinguished for interpreting the results.

The operational reference distance was defined as the greatest separation at which the packet loss percentage was equal to or lower than 50%. This threshold was adopted solely as an internal criterion for comparing the operating conditions of the prototype and does not imply fully reliable communication. In contrast, the maximum distance with detectable reception was defined as the greatest separation at which at least one packet was received, even when the link exhibited a high packet loss rate.

2.4. MATLAB Simulation

The simulation presented in this study was used as a reference to estimate the expected propagation trend of the electromagnetic link under ideal conditions. Owing to the complexity of the underwater environment, the model does not fully account for phenomena such as antenna orientation, device encapsulation, the water–air interface, or local variations in the physicochemical properties of the water. Therefore, the simulated results are used only as a reference for comparison with the experimentally observed behavior.

One of the parameters considered in the model is the electrical conductivity of the medium, which typically ranges from 300 to 1500 µS/cm in freshwater environments [15]. A conductivity value of 560 µS/cm was used in the simulation, based on the value reported for Yahuarcocha Lagoon [16]. A relative permittivity of water of 80 [17], a vacuum permittivity of 8.85x10^{-12} F/m, and a bandwidth of 125 kHz were also used, as shown in Fig. 13. Because these parameters do not represent the full spatial and temporal variability of natural environments, the model results are used solely as a theoretical reference and not as an exact prediction of the system's communication range.

```
% Physical parameters
f = 915e6; % Frequency in Hz (915 MHz)
d = [0.1, 1:0.5:15]; % distance
c = 3e8; % Speed of light in m/s
Pt_dBm = 21; % Transmission power in dBm
Pt = 10^((Pt_dBm - 30)/10); %Conv. dBm to Watts
epsilon_r = 80; % Relative permittivity
sigma = 560e-6; % Conductivity for freshwater
epsilon_0 = 8.85e-12; % Vacuum permittivity
omega = 2 * pi * f; % Angular frequency
```

Fig. 13. *Data variables used for simulation.*
Source: *own elaboration.*

Because water absorbs electromagnetic waves as a consequence of the electrical conductivity (σ) of the medium, this absorption can be modeled using the attenuation constant (α), expressed in nepers per meter (Np/m). Equation (2) is used to calculate the attenuation constant in highly lossy media [18]. The

RCTA
Revista Colombiana de Tecnologías de Avanzada
UNIPAMPLONA

parameters considered include the angular frequency (2πf), the permittivity of the medium (ε), the electrical conductivity of the medium (σ), and the operating frequency (f).

$$\alpha = \frac{\omega}{c}\sqrt{\frac{\varepsilon_r}{2}\left(\sqrt{1+\left(\frac{\sigma}{\varepsilon_0 \omega}\right)^2}-1\right)} \quad (2)$$

Another important parameter considered in the simulated environment is the SNR at different distances. For this purpose, (3) is used, which represents the general expression for calculating the thermal noise power in a communication system [18]. The equation considers parameters such as the system noise figure (NF), the Boltzmann constant (k), the equivalent noise temperature (T), and the bandwidth (B).

$$N_0 = (NF)kTB \quad (2)$$

2.5. Test Environments

The functional validation was conducted in three aquatic scenarios. The first scenario consisted of a swimming pool measuring 12 m in length and 6.5 m in width. For the comparison presented in Table 3, the sensor node antenna was positioned at a depth of 0.8 m relative to the buoy antenna, while the horizontal distance was progressively increased from 1 m until packet reception was lost. The horizontal distance was measured along the water surface between the vertical projection of the sensor node position and the location of the buoy, as shown in Fig. 14.

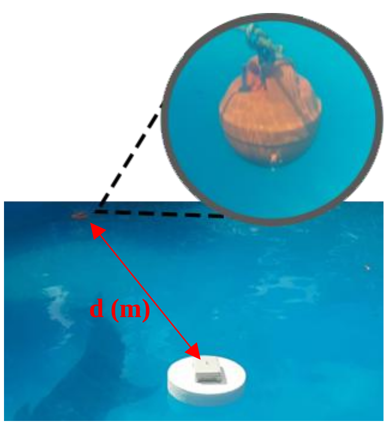

Fig. 14*. Experimental environment in a swimming pool.*
Source: *own elaboration.*

The second scenario corresponded to Yahuarcocha Lagoon, located in Ibarra, Imbabura Province. This body of water was selected because of its turbidity conditions and the reference conductivity value reported in [16]. The tests maintained the UW2OW configuration and the horizontal measurement procedure used in the swimming pool, while evaluating sensor node depths of 0.25, 0.5, and 0.8 m, as shown in Fig. 15.

Fig. 15*. Experimental environment at Yahuarcocha Lagoon.*
Source: *own elaboration.*

The third scenario corresponded to San Pablo Lagoon, located in Imbabura Province near the city of Otavalo, Ecuador. This environment was selected because it exhibited visual turbidity conditions different from those observed in Yahuarcocha Lagoon. The tests were conducted using the same UW2OW configuration, the same sensor node depths, and the same horizontal distance measurement procedure applied in the previous scenarios, as shown in Fig. 16.

(a) *(b)*
Fig. 16*. Experimental environment at San Pablo Lagoon. Communication buoy suspended on the water Surface (a) and submerged sensor node (b),*
Source: *own elaboration.*

3. RESULTS

The results are presented in three sections. First, the results obtained from the reference model implemented in MATLAB are presented.

RCTA
Revista Colombiana de Tecnologías de Avanzada
UNIPAMPLONA

Subsequently, the measurements collected during the functional validation of the system in the swimming pool and in Yahuarcocha and San Pablo Lagoons are reported. Finally, the storage and visualization of the environmental data through Firebase and the web platform are verified. The simulation and experimental measurements are analyzed as complementary elements, without assuming that the theoretical model exactly reproduces the conditions of the natural environments.

3.1. Simulation Results

The estimated received power and signal-to-noise ratio as functions of distance are presented in Fig. 17. For the SF12 configuration with a bandwidth of 125 kHz, a nominal sensitivity of −137 dBm was used as a reference [20]. This value corresponds to the theoretical performance of the transceiver under controlled conditions and does not directly represent the effective sensitivity of the complete prototype in the experimental scenarios.

The evaluated distances range from 0.1 m, corresponding to the depth of the antenna installed on the communication buoy, to a maximum separation of 15 m between the two nodes. Under the assumptions adopted in the simulation, the estimated received power crosses the nominal sensitivity threshold at approximately 12.5 m, as shown in Fig. 17(a). Therefore, this distance represents only a theoretical reference derived from the model. It should not be interpreted as the guaranteed practical range of the system because the simulation does not fully account for losses caused by the antenna, device encapsulation, the water–air interface, antenna orientation, environmental noise, and variability in the aquatic medium.

The simulated SNR decreases with distance until it approaches −20 dB, as shown in Fig. 17(b). This value is used as a reference for interpreting link degradation; however, practical reception depends on the combined effects of RSSI, SNR, packet loss, and the physical conditions of the system. Consequently, the simulation provides an indication of the expected propagation trend, whereas the operational distance must be determined from the functional validation tests.

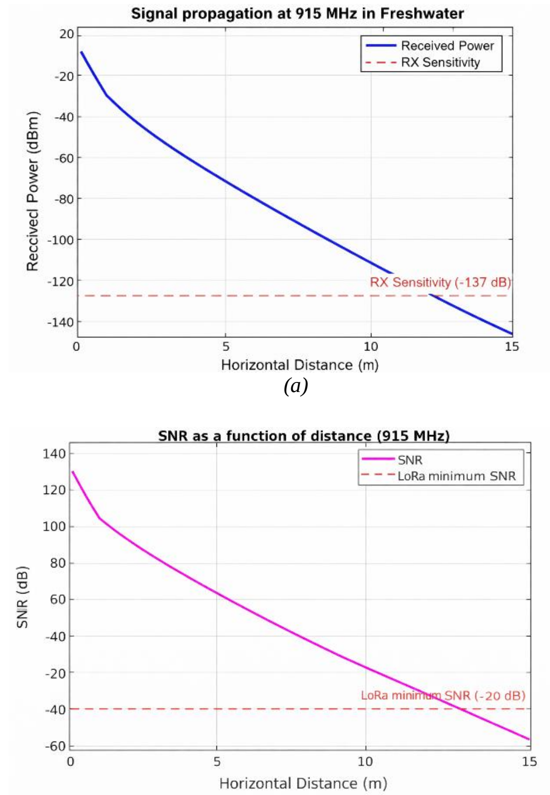

(a)

(b)

Fig. 17. *Signal propagation graphs at 915 MHz. Received signal power graph (a) and signal-to-noise ratio graph (b).* ***Source:*** *own elaboration.*

3.2. Test Environment Results

For the functional validation of the system, a fixed configuration of SF12, a bandwidth of 125 kHz, and CR 4/8 was maintained. SF12 was selected because of its high nominal sensitivity [20] and its suitability for robust, low-data-rate links. This study does not include an experimental comparison among different Spreading Factor values because its objective is to verify the operation of the complete architecture under a constant configuration. The distances were measured horizontally along the water surface, from the vertical projection of the submerged node position to the location of the buoy.

Table 3 summarizes the metrics obtained during the functional validation of the system at a depth of 0.8 m in the swimming pool and in San Pablo and Yahuarcocha Lagoons. For each scenario, the table presents the maximum distance with detectable reception, the operational reference distance, the number of transmitted and received packets, packet loss, RSSI, SNR, and delay.

Table 3: *Communication tests with a sensor node depth of 0.8 m in the three evaluated environments*

	Pool	L. SP	L. YAH
Maximum distance with detectable reception	11.4 m	4.5 m	1.2 m
Operational reference distance	10 m	3.5 m	0.8 m
Packets transmitted at the maximum distance N_{tx}	100	100	100
Packets received at the maximum distance N_{rx}	16	16	3
Packet loss at the maximum distance	84%	84%	97%
Packet loss at the operational reference distance	30%	50%	40%
Mean RSSI ± standard deviation at the maximum distance	−116 ± 0.5 dBm	−116 ± 0.45 dBm	−116 ± 0.38 dBm
Mean SNR ± standard deviation at the maximum distance	−20 ± 1.33 dB	−18 ± 2.27 dB	−18 ± 0.6 dB
Mean delay ± standard deviation at the maximum distance	5942 ± 532 ms	6237 ± 598 ms	5650 ± 504 ms

Source: *own elaboration.*

At a depth of 0.8 m, the maximum distance with detectable reception was 11.4 m in the swimming pool, 4.5 m in San Pablo Lagoon, and 1.2 m in Yahuarcocha Lagoon. However, packet loss increased considerably near these distances in all three scenarios. Therefore, these maximum values represent marginal reception conditions rather than reliable operating distances. The operational reference distances were shorter and were established according to the criterion defined in the methodology.

Table 4 presents the metrics recorded at a depth of 0.5 m in San Pablo and Yahuarcocha Lagoons. The results are interpreted by distinguishing between the marginal reception observed at the maximum distance and system operation at the operational reference distance.

Table 4: *Communication tests with a sensor node depth of 0.5 m in San Pablo and Yahuarcocha Lagoons*

	L. SP	L. YAH
Maximum distance with detectable reception	7 m	4 m
Operational reference distance	5.5 m	3.5 m
Packets transmitted at the maximum distance N_{tx}	100	100
Packets received at the maximum distance N_{rx}	36	15
Packet loss at the maximum distance	64%	85%
Packet loss at the operational reference distance	42%	46%
Mean RSSI ± standard deviation at the maximum distance	−116 ± 0.52 dBm	−116 ± 0.58 dBm
Mean SNR ± standard deviation at the maximum distance	−17 ± 1.68 dB	−22 ± 2.65 dB
Mean delay ± standard deviation at the maximum distance	6310 ± 505 ms	5398 ± 493 ms

Source: *own elaboration.*

At a depth of 0.5 m, detectable reception was achieved up to 7 m in San Pablo Lagoon and 4 m in Yahuarcocha Lagoon. SNR values close to or below −20 dB were associated with marginal link conditions and high packet loss rates. Consequently, the occasional reception of packets was not interpreted as continuous or stable communication.

Table 5 summarizes the metrics obtained at a depth of 0.25 m in San Pablo and Yahuarcocha Lagoons. This depth yielded the greatest distances with detectable reception among the natural scenarios; however, link reliability decreased as these maximum distances were approached.

Table 5: *Communication tests with a sensor node depth of 0.25 m in San Pablo and Yahuarcocha Lagoons*

	L. SP	L. YAH
Maximum distance with detectable reception	13 m	8.5 m
Operational reference distance	12 m	7.5 m
Packets transmitted at the maximum distance N_{tx}	100	100
Packets received at the maximum distance N_{rx}	27	2
Packet loss at the maximum distance	73%	98%
Packet loss at the operational reference distance	47%	36%
Mean RSSI ± standard deviation at the maximum distance	−116 ± 0.4 dBm	−116 ± 0.5 dBm

Mean SNR ± standard deviation at the maximum distance	−18 ± 2.5 dB	−23 ± 1.5 dB
Mean delay ± standard deviation at the maximum distance	6403 ± 792 ms	5592 ± 485 ms

Source: *own elaboration.*

At a depth of 0.25 m, the greatest distances with detectable reception in the natural scenarios were recorded: 13 m in San Pablo Lagoon and 8.5 m in Yahuarcocha Lagoon. However, packet loss rates of 73% and 98%, respectively, indicate that these distances correspond to the reception limit of the system. According to the stability criterion defined for the application, the operational reference distances were reduced to 12 m and 7.5 m, respectively.

Under the evaluated conditions, decreasing the depth was accompanied by an increase in the distance with detectable reception. Nevertheless, the differences among the scenarios cannot be attributed exclusively to turbidity, since other factors may also influence link performance, including electrical conductivity, antenna orientation, water movement, device encapsulation, and environmental noise. The mean delays ranged from approximately 5 to 6.4 s; therefore, their effect is analyzed in Section 4.

The means and standard deviations were calculated exclusively from the successfully received packets. Under conditions in which only a small number of packets were received, these values are presented for descriptive purposes only and do not support statistical inferences regarding the overall behavior of the link.

3.3. Validation of Data Storage and Visualization

The data acquired by the sensors were transmitted to the communication buoy and subsequently stored in Firebase for visualization through the web platform. Fig. 18 presents the temporal evolution of the pH values (Fig. 18(a)) and turbidity measurements (Fig. 18(b)) recorded during the tests. These plots were used to verify the continuity of the information flow among the sensor node, the communication buoy, the database, and the user interface.

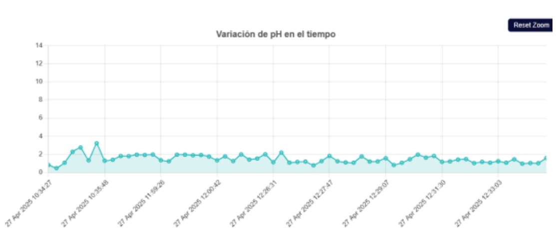

(a)

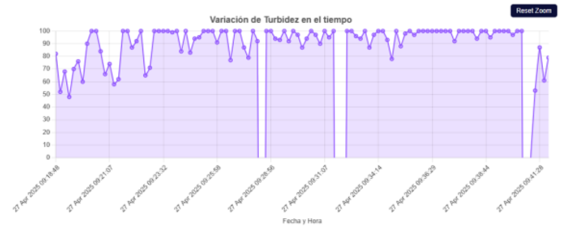

(b)

Fig. 18*. Temporal evolution of the pH sensor data (a) and turbidity sensor data (b).*
Source: *own elaboration.*

The web platform enabled verification of the reception, storage, and visualization of the data transmitted by the system. Fig. 19 displays, through data cards, the RSSI, SNR, packet number, delay, payload size, battery level, and timestamp of the most recent update. This validation confirms the functional integration among the sensor node, the communication buoy, Firebase, and the web interface.

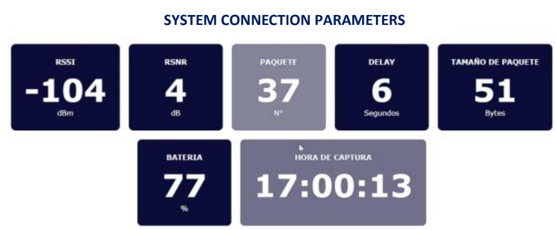

Fig. 19*. Real-time data obtained from the web platform through Firebase.* ***Source:*** *own elaboration.*

4. DISCUSIÓN

The validation process confirmed the functional integration of the sensor node, the LoRa–Wi-Fi buoy, Firebase, and the web platform across the three evaluated scenarios. The system successfully received and displayed environmental information transmitted from a submerged node; however, the communication range and continuity of reception varied according to depth and test environment. Therefore, the results should be interpreted as an operational validation of the prototype rather than as a generalizable model of the underwater channel.

The approximate distance of 12.5 m obtained from the MATLAB simulation was of the same order of magnitude as some of the maximum distances recorded experimentally. Nevertheless, this similarity does not constitute an exact validation of the model. The simulation assumes simplified conditions and reference parameters, whereas the experimental measurements include additional losses caused by device encapsulation, antennas, orientation, the water–air interface, and environmental variability. Consequently, the model is used only to compare the general attenuation trend.

The difference between the nominal sensitivity of −137 dBm and the value close to −116 dBm observed before the practical loss of the link arises because these two quantities represent different conditions. The former corresponds to the nominal sensitivity of the transceiver for SF12 and a bandwidth of 125 kHz under controlled conditions. The latter represents an empirical threshold of the complete prototype in the evaluated scenarios. Losses introduced by the enclosure, antenna, impedance matching, orientation, contact with water, and the water–air interface reduce the available link margin. Therefore, −116 dBm is not proposed as a universal LoRa threshold, but rather as a value observed for the developed implementation.

increases the duration of each symbol and, consequently, the packet time on air. In addition, the Coding Rate of 4/8, the 125 kHz bandwidth, the 12-symbol preamble, the payload size, and the processing performed by the devices contribute to the total delay. These delays may be acceptable for the periodic monitoring of slowly varying environmental parameters, such as pH and turbidity, but they limit the use of the system in real-time control applications.

Packet loss rates above 60% recorded near the maximum distances highlight the need to distinguish between the maximum distance with detectable reception and the operational distance. The maximum distances represent the limits at which information could still be received, whereas the operational distances correspond to more conservative deployment conditions. Future implementations could incorporate local storage, retransmissions, reception acknowledgments, and temporal redundancy; however, these mechanisms were not evaluated in the present study.

Table 6: *Comparative analysis between the proposed work and related studies*

	Proposed System	433 MHz Tests [5]	2.4 GHZ Tests [3]	2.4 GHZ Tests [4]
Test Environment	Swimming pool and two lagoon environments	Pool	Pool	Aquarium
Technology Used	LoRa	TWS-433	Wifi	Wifi y Bluetooth
Measurement Method	UW2OW (Submerged node and surface node)	OW2OW (Both nodes on the surface)	UW2UW (Both nodes on the surface)	UW2OW (Submerged node inside aquarium and surface node)
Evaluated Depth	0.25, 0.5 y 0.8 m	Surface level	15 cm	Surface level (15 cm)
Maximum Achieved Distance	11.4 m (Pool) 13 m (San Pablo L.) 8.5 m (Yahuarcocha L.)	9 m	16 cm	19 cm (Wifi) 18 cm (Bluetooth)
Observed Empirical RSSI Threshold	−116 dBm	−116 dBm	Not reported	−89 dBm
Additional Evaluated Factors	RSNR Dalay Packet loss	Attenuation, free-space propagation	RTT, received packets	Saltwater conditions

Source: *own elaboration.*

SNR values close to or below −20 dB should be interpreted as marginal reception conditions. The robustness of the modulation scheme and the error-correction mechanism may allow occasional packet reception under these conditions; however, the high packet loss rates indicate that the link does not remain stable. Therefore, the reception of one or several packets at the communication limit is insufficient to consider a given distance reliable.

The mean delays, ranging from approximately 5 to 6.4 s, correspond to the interval measured between packet transmission at the sensor node and packet reception at the communication buoy. These values are mainly associated with the LoRa configuration selected to improve link robustness. The use of SF12

Related studies show that the range of underwater electromagnetic communications depends on the operating frequency, link configuration, depth, and test medium, as summarized in Table 6. The proposed system is primarily distinguished by the integration of a sensor node, a LoRa–Wi-Fi buoy, cloud storage, and a web platform within a functional architecture. Distance comparisons should be interpreted with caution because the studies employ different antennas, frequencies, link geometries, and aquatic conditions.

The limitations of this study include the use of a single LoRa configuration during the reported validation, the absence of a complete electromagnetic characterization of the antennas within the enclosure, the use of reference physicochemical parameters in the simulation, and the uncontrolled variability of the natural environments. Consequently, the results are valid for the developed prototype and the evaluated conditions but should not be directly extrapolated to other bodies of water.

5. CONCLUSIONS

This study enabled the design, implementation, and functional validation of a short-range underwater monitoring architecture comprising a submerged sensor node, a LoRa–Wi-Fi communication buoy, a cloud database, and a web platform. The prototype successfully acquired, transmitted, stored, and displayed environmental information in both controlled and natural freshwater environments.

The validation results showed that depth and the specific conditions of each scenario affected both the maximum distance with detectable reception and link continuity. The maximum distances did not necessarily represent reliable operation because high packet loss rates were recorded near the reception limit. Therefore, system deployment should be based on conservative operational distances, considering that the effective threshold of the complete system may differ from the nominal sensitivity of the transceiver.

The selected configuration produced delays of several seconds; therefore, the architecture is suitable for the periodic monitoring of slowly varying environmental parameters but not for real-time control applications. Future work will focus on optimizing the enclosure and antenna system, incorporating local data storage and retransmission mechanisms, and evaluating communication strategies to extend coverage. These alternatives must be experimentally validated before their feasibility can be confirmed.

Author Contributions: conceptualization: Jaime Michilena-Calderón and Fabián Cuzme-Rodríguez; methodology: Jaime Michilena-Calderón and Fabián Cuzme-Rodríguez; software: Diego. Montezuma-Rosero; validation: Fabián Cuzme-Rodríguez, Jaime Michilena-Calderón and Luis Suárez-Zambrano; formal analysis: Diego Montezuma-Rosero and Fabián Cuzme-Rodríguez; investigation: Diego Montezuma-Rosero; resources: Jaime Michilena-Calderón and Luis Suárez-Zambrano; data curation: Fabián Cuzme-Rodríguez; writing—original draft: Diego A. Montezuma-Rosero; writing—review and editing: Fabián Cuzme-Rodríguez, Jaime Michilena-Calderón and Luis Suárez-Zambrano; visualization: Diego Montezuma-Rosero; supervision: Jaime Michilena-Calderón; administration: Jaime Michilena-Calderón; funding acquisition: Diego Montezuma-Rosero. All authors have read and approved the final version of the manuscript.

Funding: The authors declare that the development of this research work did not receive any type of public or private funding, nor is it part of any financially supported project.

Materials and Data Availability: Data available on GitHub:
https://github.com/ArbeyCr/LoRa_Subacuatico

Acknowledgments: The authors thank Universidad CESMAG, Colombia, where the preliminary advances of this work were presented during the 3rd SAFARIS TECH INTERNATIONAL Congress 2025. The present manuscript extends that initial version through the complete implementation of the architecture, its validation in aquatic environments, and a discussion of its operational limitations. The authors also thank the Renewable Natural Resources program at Universidad Técnica del Norte, Ecuador, for providing laboratory facilities for sensor calibration; Fernando Guerra Goyes for providing the Ubiquiti Loco M2 antenna; and Franco Elías Montezuma and Grace Gisel Cuasqui for their assistance during the experimental tests. MATLAB R2025a was used to implement the reference simulation model.

REFERENCES

[1] S. Ruiz and M. Muñoz, "Análisis de propagación de las comunicaciones ópticas subacuáticas.," Escuela Superior Politécnica de Chimborazo, Jul. 2022, doi: 10.47187/perspectivas.5.2.200.

[2] F. Cuzme Rodríguez, A. Velasco Suárez, M. Domínguez Limaico, L. Suárez Zambrano, H. Farinango Endara, and M. Mediavilla Valverde, "Application for the Study of Underwater Wireless Sensor Networks: Case Study," Lecture Notes in Networks and Systems, vol. 619 LNNS, pp. 124–136, 2023, doi: 10.1007/978-3-031-25942-5_11.

[3] C. S. Sendra, "'Comunicaciones inalámbricas subacuáticas a 2,4 GHz para la transmisión de datos con altas tasas de transferencia' TRABAJO FINAL DE GRADO,"

Universidad Politecnica de Valencia, Jan. 2011, Accessed: Aug. 04, 2024. [Online]. Available: https://riunet.upv.es/handle/10251/14605

[4] R. A. Arias, "Caracterización de sistemas de comunicación RF y ópticos en aplicaciones submarinas," Universidad Politécnica de Catalunya BarcelonaTech, Jul. 2022, Accessed: Aug. 04, 2024. [Online]. Available: https://upcommons.upc.edu/handle/2117/372768

[5] M. Delgado, S. Chango, and Benavidez. Mateo, "Uso de la banda de 433MHz para comunicaciones subacuáticas en ambientes controlados," Universidad de las Fuerzas Armadas (ESPE), vol. 14, no. 2, pp. 1–6, Mar. 2024, doi: 10.24133/MASKAY.V14I2.3176.

[6] D. A. Jiménez Ballart, "Estudio de la cobertura de la modulación LoRa en la banda de 915[Mhz] en un ambiente urbano," Universidad de Chile, Santiago de Chile, 2018. Accessed: Mar. 10, 2025. [Online]. Available: https://repositorio.uchile.cl/handle/2250/168163

[7] H. M. Calero, "Red sensores multiservicio LPWAN LoRa, LoRaWAN, TTN y MQTT," Universitat Oberta de Catalunya, Jan. 2023, Accessed: Aug. 04, 2024. [Online]. Available: https://openaccess.uoc.edu/bitstream/10609/147334/6/caleroherruzo20TFM0123memoria.pdf

[8] F. Cuzme-Rodríguez, P. Otero, M. Á. Luque-Nieto, M. Domínguez-Limaico, and H. Farinango-Endara, "Underwater Wireless Sensor Networks and Cryptographic Applications," Communications in Computer and Information Science, vol. 1648 CCIS, pp. 46–58, 2022, doi: 10.1007/978-3-031-18272-3_4.

[9] K. Lin, T. Hao, W. Zheng, and W. He, "Analysis of lora link quality for underwater wireless sensor networks: A semi-empirical study," Asia-Pacific Microwave Conference Proceedings, APMC, vol. 2019-December, pp. 120–122, Dec. 2019, doi: 10.1109/APMC46564.2019.9038666.

[10] A. Dala and T. Arslan, "Design, Implementation, and Measurement Procedure of Underwater and Water Surface Antenna for LoRa Communication," Sensors 2021, Vol. 21, Page 1337, vol. 21, no. 4, p. 1337, Feb. 2021, doi: 10.3390/S21041337.

[11] A. Pozzebon, I. Cappelli, F. Campagnaro, R. Francescon, and M. Zorzi, "LoRaWAN Transmissions in Salt Water for Superficial Marine Sensor Networking: Laboratory and Field Tests," *Sensors*, vol. 23, no. 10, Art. no. 4726, 2023, doi: 10.3390/s23104726.

[12] Heltec, "HTIT-WB32LA_V3 LoRa Node Development Kit," Heltec Automation, vol. 1.1, Sep. 2022, Accessed: Apr. 12, 2024. [Online]. Available: https://heltec.org

[13] Firebase, "Firebase Realtime Database," Firebase. Accessed: Apr. 06, 2025. [Online]. Available: https://firebase.google.com/docs/database?hl=es-419

[14] M. Serrano, "¿Qué es la protección IP65? ¿En qué se diferencia con IP67? - IkolCrane," IkoCrane. Accessed: May 19, 2025. [Online]. Available: https://www.ikolcrane.com/aprender/que-es-la-proteccion-ip65

[15] S. J. Carrasquero, J. C. Marín, C. Muñoz, R. Vargas, C. Vargas, and P. Tuviñez, "Parámetros químicos medidos en las aguas de piscinas de los dos... | Download Scientific Diagram," ResearchGate, vol. 56, Jan. 2016, Accessed: Mar. 22, 2025. [Online]. Available: https://www.researchgate.net/figure/Parametros-quimicos-medidos-en-las-aguas-de-piscinas-de-los-dos-complejos-recreacionales_fig1_325654330

[16] J. Pabón, "Distribución y evaluación de la vegetación macrofítica en el lago de Yahuarcocha, Provincia de Imbabura," Universidad Técnica del Norte, Recursos Naturales Renovables, Dec. 2015, Accessed: Mar. 01, 2025. [Online]. Available: https://repositorio.utn.edu.ec/handle/123456789/6943

[17] S. O. Nelson, "Dielectric Properties of Agricultural Products: Measurements and Applications," IEEE Transactions on Electrical Insulation, vol. 26, no. 5, pp. 845–869, 1991, doi: 10.1109/14.99097.

[18] F. T. Ulaby and U. Ravaioli, FUNDAMENTALS OF APPLIED ELECTROMAGNETICS Eighth Edition. Pearson Education, 2023. Accessed: Mar. 22, 2025. [Online]. Available: www.pearsoned.com/permissions/.

[19] E. Navarro, "Desarrollo de un simulador de radar de apertura sintética y propuesta de diseño de radio frecuencia.," Esuela Técnica Superior de Ingeniería y Sistemas de Telecomunicaciones, 2017. Accessed: Mar. 23, 2025. [Online]. Available: https://oa.upm.es/52922/1/TFG_EDUARDO_NAVARRO_SABARIEGOS.pdf

[20] Semtech, "SX1261/2 Long Range, Low Power, Sub-GHz RF Transceiver," Datasheet.

Accessed: Apr. 12, 2024. [Online]. Available: https://semtech.my.salesforce.com/sfc/p/#E0000000JelG/a/2R000000Un7F/yT.fKdAr9ZAo3cJLc4F2cBdUsMftpT2vsOICP7NmvMo

[21] A. Jaszczyszyn, A. G. Jaszczyszyn, M. Guiguet, and H. D. Ramón, “Comparación de una red LoRaWAN con modelos de propagación en un entorno con vegetación de soja,” Elektron, vol. 8, no. 2, pp. 101–106, Dec. 2024, doi: 10.37537/rev.elektron.8.2.203.2024.